



Rapid Melt Growth of Germanium Tunnel Junctions

Jialin Zhao, Alan C. Seabaugh,^z and Thomas H. Kosel

Department of Electrical Engineering, University of Notre Dame, Notre Dame, Indiana 46556-5637, USA

A rapid melt growth process for forming interband n + p+ Esaki tunnel junctions on Ge is shown. The process uses a phosphorus spin-on diffusant and rapid thermal annealing to form the n+ side of the junction, while for the p+ side, a deposited aluminum film serves both as an acceptor dopant source and a melt for epitaxial regrowth of p + Ge. The current density in these junctions depends strongly on the peak temperature of the Al–Ge melt and ranges between a few $\mu\text{A}/\mu\text{m}^2$ to over $1 \text{ mA}/\mu\text{m}^2$. The use of a silicon nitride microcrucible improves the surface morphology by confining the melt. Record forward peak current density of $1.2 \text{ mA}/\mu\text{m}^2$ and reverse interband tunnel current density of $3.8 \text{ mA}/\mu\text{m}^2$ is achieved at a peak temperature of approximately 600°C .

© 2007 The Electrochemical Society. [DOI: 10.1149/1.2728734] All rights reserved.

Manuscript submitted July 21, 2006; revised manuscript received February 12, 2007. Available electronically April 23, 2007.

Interest in germanium technology has been rekindled in recent years for metal oxide semiconductor field-effect transistors,¹ photodetectors,² and nanowires.³ This paper discusses a method for forming shallow, abrupt, heavily doped, p-type layers in Ge with particular application to the formation of Esaki p + n+ tunnel junctions. The rapid melt growth technique described here is also relevant to Ge p+ contact formation in devices where implantation cannot be used due to thermal limits. The ability to form high-current-density tunnel junctions is a central requirement in low-power-dissipation field-effect tunnel-transistors⁴ and in circuits combining transistors and tunnel diodes.⁵

To achieve high current-density in tunnel junctions requires formation of the highest possible p and n doping densities with the maximum doping abruptness (steepest possible slope of the doping concentration at the junction). High doping abruptness and doping density are needed to maximize interband tunneling current. In Ge, the p dopant with the highest solid solubility is Al, exceeding $2 \times 10^{20} \text{ cm}^{-3}$ in the temperature range $600\text{--}700^\circ\text{C}$.⁶ Interdiffusion of the dopant elements across the interface should be minimized to achieve the most abrupt doping profile. Hence, in this work a rapid melt growth technique has been explored, to minimize the time available for interdiffusion of the dopants across the junction.

The use of rapid thermal growth techniques for recrystallizing deposited Ge from crystalline Si seeds has shown that both lateral and vertical crystallization can be achieved with high growth velocities (in m/s) driven by rapid thermal processors.^{7–9} In this work, the rapid melt growth technique is extended by the introduction of Al over the Ge to act as both an acceptor dopant and as a melt to dissolve and regrow an abrupt p+ on n+ junction. This approach stems from early Ge bipolar transistor manufacturing, where pellets of In or Pb were placed on Ge wafers and used for melt-back and regrowth of pnp Ge transistor junctions.¹⁰

The In–Ge and Pb–Ge alloy systems have simple eutectic binary phase diagrams with relatively low eutectic temperatures. Annealing above the eutectic temperature first dissolved some Ge into the liquid phase, and then solidified a doped Ge layer during cooling, which formed the collector or emitter of the transistor. The remainder of the liquid then formed a solid eutectic mixture which acted as a soft metal alloy contact on the surface. Soft metals were used to reduce mechanical stresses when contact wires were attached. In these alloy junction processes, heating and cooling rates were typically around $0.5^\circ\text{C}/\text{s}$ with a peak annealing temperature of 550°C .¹⁰ In the present work, heating and cooling rates were increased by more than two orders of magnitude to $100\text{--}150^\circ\text{C}/\text{s}$, to achieve high dopant abruptness. At these high rates, the regrowth time is reduced from approximately 1000 s to around 4, decreasing the dopant diffusion length (\sqrt{Dt}) during solidification by approximately 15 times.

Approach

The metallurgical principles of our process can be described with the aid of the simple eutectic Al–Ge phase diagram¹¹ of Fig. 1. Upon heating Al in contact with Ge to the eutectic temperature $T_E = 420^\circ\text{C}$, Al and Ge would be expected to react to form a liquid with a Ge weight percentage of 51.6%. Above the eutectic temperature, the weight percentage of Ge in the Al increases along the liquidus line until a peak temperature is reached. Upon cooling from the peak anneal temperature, Ge solidifies from the melt, and (as in Ref. 10) this should be expected to occur epitaxially on the pre-existing Ge surface. The regrown Ge epi layer is degenerately p+ doped, because its Al content should follow the solubility line separating the L + Ge and solid Ge regions; solubility increases as the alloy cools. Especially during rapid cooling, it should be a good approximation to assume no Al diffusion in the solid Ge, so the first regrown Ge (which defines the junction) would have a lower Al content than the last. Precipitation of Ge during cooling drives the liquid composition of the melt along the liquidus line, reaching the eutectic composition at T_E , when a eutectic mixture of Al rich and Ge rich phases solidify. The temperature at which the eutectic reaction occurs will likely be lower during rapid cooling, but the p + n+ junction should not be affected by this. The liquid composition attained at the maximum temperature of the process may also differ from that given by the phase diagram.

A schematic description of the tunnel junction process is shown in Fig. 2. Germanium p-type (100) Czochralski substrates were used, with resistivity of $0.18\text{--}0.19 \Omega \text{ cm}$. Wafers were degreased in acetone and methanol followed by removal of the native oxide in a

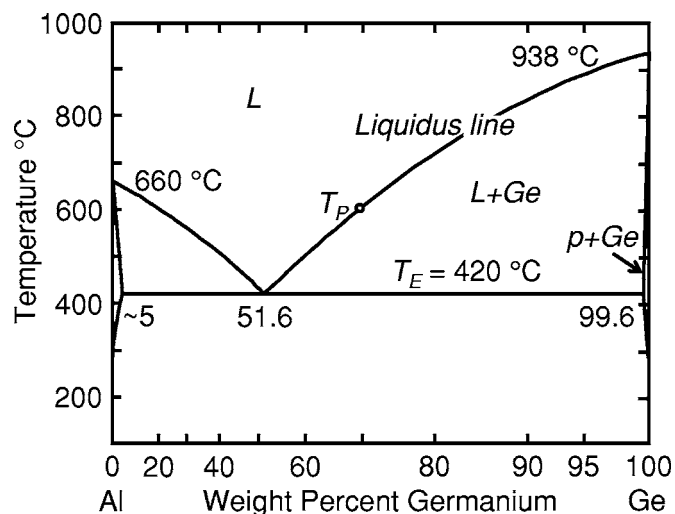


Figure 1. Al–Ge phase diagram after Okamoto.¹¹

^z E-mail: seabaugh.1@nd.edu

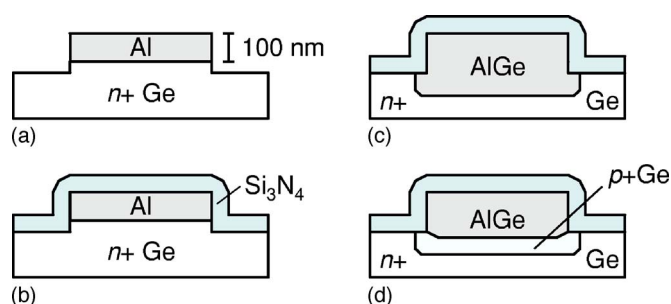


Figure 2. (Color online) Schematic device cross section of the rapid melt growth process drawn to scale in the vertical direction. (a) Germanium is doped n+ by rapid thermal diffusion of phosphorus followed by aluminum deposition, patterning, and etching. (b) A plasma nitride cap is applied. (c) At the peak anneal temperature (600°C in this example) an AlGe melt forms with a meltback of 110 nm. (d) On cooling, a heavily doped p + Ge layer is grown; on cooling from a peak temperature of 600°C, a 60 nm layer is grown.

10:1 buffered HF etch for 25 s. The wafers were then spin coated with an Emulsitone phosphosilicate containing P at a concentration of $1 \times 10^{21} \text{ cm}^{-3}$, and subsequently baked to remove the organics at 150°C for 10 min in air. Samples were next loaded into a Modular Process Technology RTP600 rapid thermal processor. Phosphorus was diffused at 800°C for 300 s in a forming gas (95N₂:5H₂, 10 slpm) ambient under atmospheric pressure. From Hall-effect measurements, this process was found to yield an electron density of approximately $2 \times 10^{20} \text{ cm}^{-3}$. A buffered HF clean of 300 s removed the spin-on-diffusant residues prior to electron-beam evaporation of 100 nm of Al. The Al was patterned into square mesas, ranging in size from 3×3 to $20 \times 20 \mu\text{m}$, by photolithography and etching in Cyantec's Al-12 etchant (71 wt % H₃PO₄: 10 wt % CH₃COOH: 2 wt % HNO₃). The Ge was next etched to a depth of approximately 40 nm in 30% H₂O₂ using the Al metal as a mask, as shown in Fig. 2b.

Rapid melt growth (100–150°C/s) was performed in a forming gas ambient, both with and without a 50 nm thick silicon nitride (SiN) capping layer formed by plasma-enhanced chemical vapor deposition, Fig. 2b. On heating the wafer above the Al–Ge eutectic temperature of 420°C, the Al consumes an amount of Ge which depends on temperature. At the peak anneal temperature the ratio of the penetration depth, x , of the melt below the original Ge surface (defined in the inset of Fig. 3) to the deposited Al thickness, t_{Al} can be determined from the Al–Ge binary phase diagram of Okamoto¹¹ according to the relation

$$\frac{x}{t_{\text{Al}}} = \frac{\rho_{\text{Al}} W_{\text{Ge}}}{\rho_{\text{Ge}} I - W_{\text{Ge}}} \quad [1]$$

where ρ_{Al} and ρ_{Ge} are the densities in g/cm³ for Al and Ge, respectively, and W_{Ge} is the weight percent of Ge in the Al melt, given by the point on the liquidus line at T_p . This relation is plotted in Fig. 3. For a peak anneal temperature of 600°C, Ge is consumed to a depth of approximately 110 nm. Equation 1 does not account for lateral melting of the Ge, but for contact dimensions much greater than the melt-back depth, this formula provides a reasonable estimate.

From the peak temperature, cooling rates were approximately 40°C/s for 10 s through the eutectic temperature of 420°C, then cooling to under 100°C in 2 min. On cooling, a heavily Al-doped Ge layer was regrown until the eutectic temperature was reached. As computed from the phase diagram, the doping density, N_{Al} in cm⁻³, decreases linearly with increasing temperature from $4.7 \times 10^{20} \text{ cm}^{-3}$ at 420°C to $2.1 \times 10^{20} \text{ cm}^{-3}$ at 725°C, Fig. 3. As the temperature decreases below 420°C, Al rich and Ge rich phases are nucleated in roughly equal proportions, forming a eutectic mixture labeled AlGe in Fig. 2d.

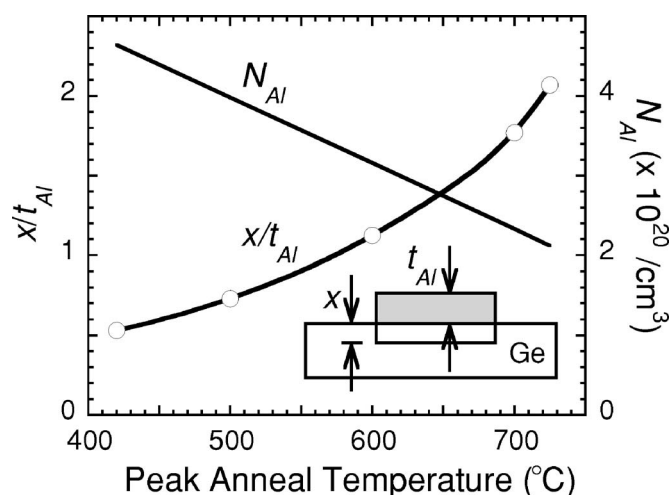


Figure 3. The ratio of the penetration depth, x , to the aluminum deposition thickness, t_{Al} as a function of peak anneal temperature, and the concentration of Al, N_{Al} in cm⁻³, as a function of the peak anneal temperature as determined from the Al–Ge binary phase diagram.¹¹

Results

The rapid melt growth process was first explored without the presence of a SiN cap during the anneal. Both anneal peak temperature and anneal time at the peak temperature were varied. The anneals were performed on a subdivided single wafer to ensure comparisons of junctions with the same phosphorus diffusion. The current voltage, I–V, characteristics for five different anneal conditions are shown in Fig. 4. The measurements are made between small and large area contacts on the top surface of the wafer as indicated in the inset of Fig. 4. The contacts are in series, and because the voltage drop across the larger device is negligible due to

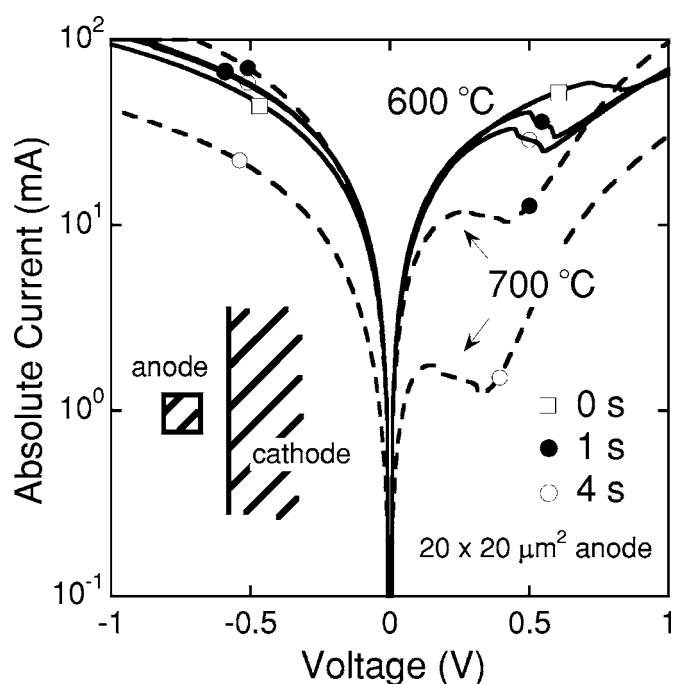


Figure 4. Dependence of Ge tunnel diode current-voltage characteristics on rapid melt growth anneal condition. The silicon nitride cap was omitted for this set of anneals. Solid lines are used for the 600°C anneals and dashed lines for the 700°C anneals; the symbols in the legend and on the curves indicate the hold time at the peak anneal temperature.

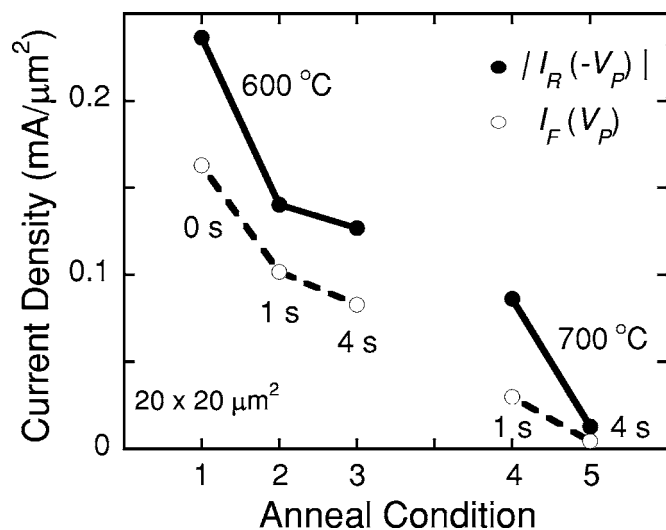


Figure 5. Dependence of current density in the forward, I_F , and reverse current, I_R , directions as a function of anneal condition for the uncapped Ge diodes of Fig. 4. In the reverse direction, the current magnitude is plotted at a voltage corresponding to minus the forward peak voltage, V_p .

its area, the voltage across the smaller device can be assumed to be equal to the applied voltage. The characteristic negative differential resistance of the tunnel junction is clearly observed for all anneal conditions and the reverse Zener tunneling characteristic is also apparent in each device. The series resistance (less than 10Ω) is responsible for the curvature at high currents; this series resistance is reasonable given the sheet resistance of the phosphorus diffusion ($9 \Omega/\square$) and the device geometry.

The peak forward current density, I_F , measured at the peak voltage, V_p , is plotted as a function of anneal condition in Fig. 5. The peak current density decreases monotonically with increasing temperature and time. This change is consistent both with the expected decrease in the junction doping with increasing temperature, Fig. 3, and the expected broadening of the dopant slope with temperature due to interdiffusion of phosphorus and aluminum at the junction. Both of these changes decrease the tunneling probability and tunnel current density, which is what is observed. Also plotted in Fig. 5 is the reverse Zener tunneling current density corresponding to a reverse voltage with an absolute magnitude equal to the forward peak voltage. At this voltage, the reverse current density should exceed the forward current density because of the greater overlap of available states for tunneling in the reverse direction over the forward direction, and this is what is observed.

Figure 6 plots the dependence of peak-to-valley current ratio (PVR) for these diodes as a function of anneal condition. For the highest current density diode in this set, the 600°C spike anneal, a current density of $0.16 \text{ mA}/\mu\text{m}^2$ is obtained at a PVR of 1.06. The PVR in the rapid melt growth junctions for these conditions are notably lower than has been achieved previously on alloy Ge diodes, PVR of 8–9 for a current density of $0.16 \text{ mA}/\mu\text{m}^2$.¹² The low PVR is an indication of a high density of defect-states at the junction leading to a high excess current in the valley region of the I-V characteristics.¹⁵ The junction roughness likely also plays a role in the high valley current.

A 50 nm SiN cap was added to act as a microcrucible^{7,8} and hold the Al-Ge melt during the alloy process. The addition of the cap prior to annealing was found to improve the morphology of the contact following anneal by holding the Al in place and suppressing islanding. The optical micrographs in Fig. 7 show a comparison of $5 \times 5 \mu\text{m}$ devices after annealing (a) with and (b) without a SiN capping layer. The left and right thirds of each micrograph are regions that were originally covered with a continuous Al film prior to

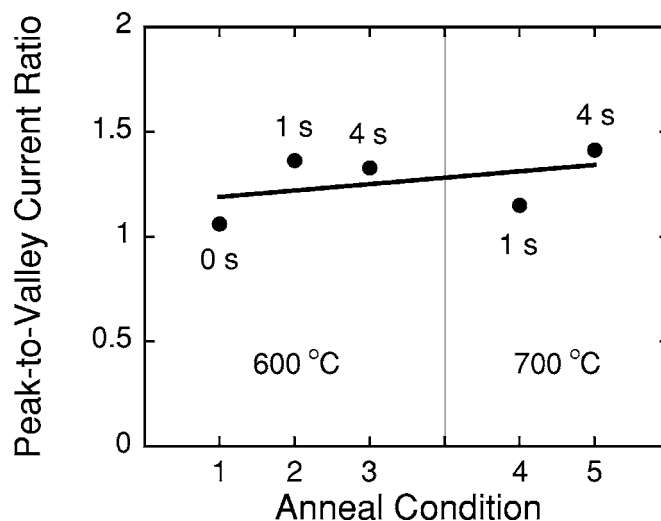


Figure 6. Peak-to-valley current ratio vs anneal condition for the uncapped Ge diodes of Fig. 5.

annealing, while the middle region contains a $5 \times 5 \mu\text{m}$ deposited Al feature surrounded by a darker Ge region. In Fig. 7a, the capping layer covered both the Al and Ge areas. The Al deposition was 100 nm thick and the anneal conditions were 440°C , 5 s, with a $100^\circ\text{C}/\text{s}$ heating rate. The fact that the dark part of the central third of the images is Ge with no Al deposit suggests that the dark regions in the metallized areas are the Ge phase of the eutectic mixture, while the white areas are the Al phase. The uncapped specimen in Fig. 7b shows large areas of Al and of Ge in both the $5 \times 5 \mu\text{m}$ feature and the larger metallized areas at the left and right, suggesting that the melt formed droplets instead of wetting the Ge. Addition of the capping layer in Fig. 7a clearly resulted in much more uniform coverage of the substrate, and the dark lines in the metallization have a typical eutectic morphology. As the size of the capped features was reduced (as small as $3 \times 3 \mu\text{m}$), the uniformity of the Al-Ge film was observed to improve and the peak current density increased (as will be shown).

With the anneal hold time set at 1 s and the same heating rate of $100^\circ\text{C}/\text{s}$, a sequence of rapid melt growths was performed on another set of wafers fabricated with the same phosphorus-diffusion conditions, but this time with a 50 nm SiN cap. The dependence of

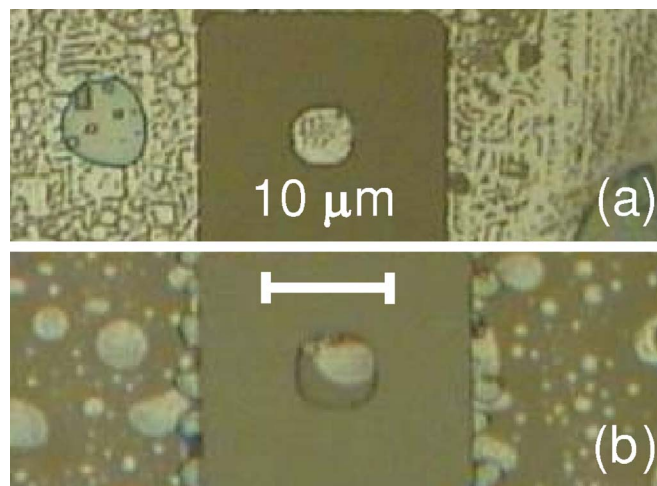


Figure 7. (Color online) Optical micrographs showing the Ge wafer surface following rapid melt growth of p + Ge at a peak temperature of 440°C : (a) capped with silicon nitride and (b) uncapped.

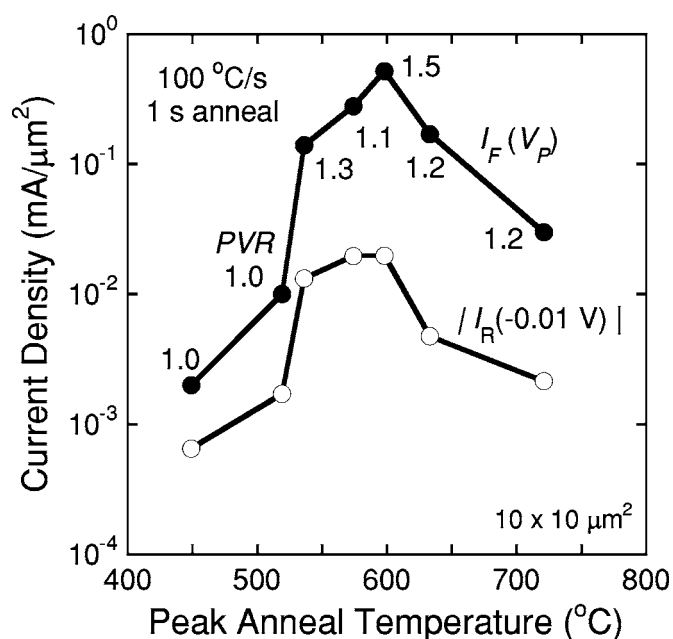


Figure 8. Germanium tunnel diode current densities vs annealing temperature with a 50 nm SiN cap. The solid circles denote measurements at the peak voltage in the forward current direction; the open circles are measurements in the reverse current direction at -0.01 V. The values for the peak-to-valley current ratio are given on the forward current curves.

forward peak current and reverse current vs anneal temperature from 440 to 725°C for these are shown in Fig. 8. In this case, a low constant reverse voltage is plotted which similarly tracks the forward-current tunneling-dependence on temperature. A maximum in the tunneling current is found at a temperature of 600°C. This current-density dependence on temperature is consistent with an improving electrical activation as temperature increases from 440 to 600°C. The decreasing tunnel current at temperatures over 600°C likely results from a degraded dopant slope, due to phosphorus diffusion into the regrown layer. Phosphorus has a diffusion length of approximately 6 nm in 1 s at 700°C and 1 nm in 1 s at 600°C in agreement with a degraded dopant slope and lower current density for anneals at 700°C and above. The Al diffusion coefficient is an order of magnitude lower than phosphorus at these temperatures. Degradation in the peak current would also result from a decrease in junction doping which, as shown in Fig. 3, decreases as peak anneal temperature is increased. Germanium tunnel diodes with a peak current density of $0.62 \text{ mA}/\mu\text{m}^2$ and PVR of 1.5 are achieved under these conditions. More than three times the current density and slightly better PVR are achieved using the SiN cap.

Germanium tunnel diodes with current densities up to $1.2 \text{ mA}/\mu\text{m}^2$ were obtained using a ramp rate of $150^\circ\text{C}/\text{s}$, an anneal condition of 600°C , a hold time of 2 s, and a SiN cap. The device current voltage characteristics are shown in Fig. 9, showing area dependence of the current density. The areas of these devices were all measured under a scanning electron microscope. As the device size was reduced the current density increased. The highest peak current density, $1.2 \text{ mA}/\mu\text{m}^2$, is achieved at the smallest junction area with reverse current density of $3.8 \text{ mA}/\mu\text{m}^2$ also achieved in this junction. The improvement in current density with reduced junction area could result from an improvement in junction morphology or an increase in edge leakage.

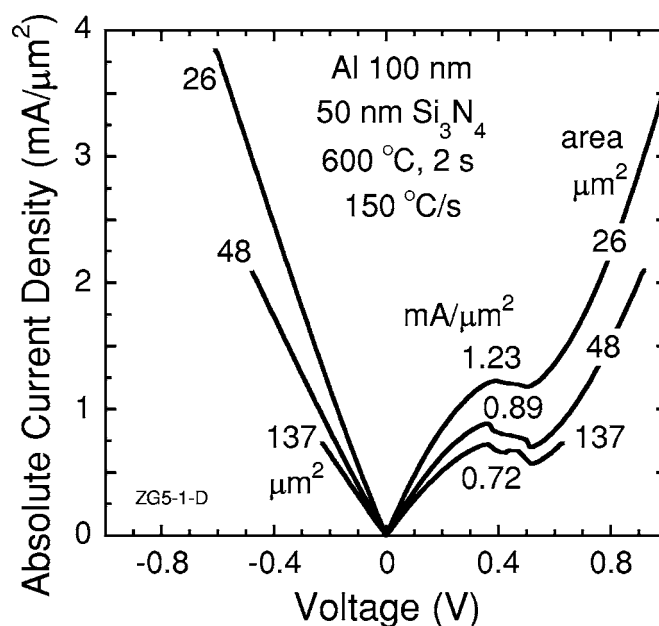


Figure 9. Current-voltage characteristics of Ge tunnel diodes with a 50 nm silicon nitride microcrucible layer and a $150^\circ\text{C}/\text{s}$ heating rate.

Conclusions

Germanium tunnel diodes with peak current densities up to $1.2 \text{ mA}/\mu\text{m}^2$ were fabricated using a rapid melt growth technique for growing heavily Al-doped p+ layers on n+ phosphorus-diffused Ge for tunnel junctions. The use of a silicon nitride cap greatly improved the surface morphology. A wide parameter space exists for raising the peak current density and reducing the valley current including optimization of the melt-back depth, optimization of the heating and cooling curves, and reduction in the device area to improve the junction uniformity.

Acknowledgments

This work was supported by the Office of Naval Research under contract N00014-02-10-924.

The University of Notre Dame assisted in meeting the publication costs of this article.

References

1. C. O. Chui, F. Ito, and K. C. Saraswat, *IEEE Trans. Electron Devices*, **53**, 1501 (2005).
2. M. Oehme, J. Werner, M. Jutzi, G. Wohl, E. Kasper, and M. Berroth, *Thin Solid Films*, **508**, 393 (2006).
3. H. Adhikari, A. F. Marshall, C. E. D. Chidsey, and P. C. McIntyre, *Nano Lett.*, **6**, 318 (2006).
4. Q. Zhang, W. Zhao, and A. Seabaugh, *IEEE Electron Device Lett.*, **27**, 297 (2006).
5. Q. Liu and A. Seabaugh, *IEEE Trans. Circuit Syst. II: Express Briefs*, **52**, 572 (2005).
6. F. A. Trumbore, *Bell Syst. Tech. J.*, **39**, 205 (1960).
7. Y. Liu, M. D. Deal, and J. D. Plummer, *Appl. Phys. Lett.*, **84**, 2563 (2004).
8. Y. Liu, M. D. Deal and J. D. Plummer, *J. Electrochem. Soc.*, **152**, G688 (2005).
9. S. Balakumar, M. M. Roy, B. Ramamurthy, C. H. Tung, G. Fei, S. Tripathy, C. Dongzhi, R. Kumar, N. Balasubramanian, and D. L. Kwong, *Electrochem. Solid-State Lett.*, **9**, G158 (2006).
10. F. J. Biondi, *Transistor Technology*, Vol. III, p. 177 and 181, D. Van Nostrand Co., New York (1958).
11. H. Okamoto, *Desk Handbook: Phase Diagrams of Binary Alloys*, p. 32, ASM International, Eden Prairie, MN (2001).
12. A. Seabaugh and R. Lake, *Tunnel Diodes*, p. 348, VCH Publishers, New York (1998).
13. A. G. Chynoweth, W. L. Feldmann, and R. A. Logan, *Phys. Rev.*, **121**, 684 (1960).